Institute of Microwave and Wireless Systems

Leibniz Universität Hannover

IEEE Transactions on Antennas and Propagation, to be published

Antenna Parameters for On-Body Communications with Wearable and Implantable Antennas

Authors:
Lukas Berkelmann
Dirk Manteuffel

DOI: 10.1109/TAP.2021.3060944

Suggested Citation:
L. Berkelmann and D. Manteuffel, “Antenna Parameters for On-Body Communications with Wearable and Implantable Antennas”, *IEEE Transactions on Antennas and Propagation, to be published*, 2021

This is an author produced version, the published version will be available at http://ieeexplore.ieee.org/

©2021 IEEE Personal use of this material is permitted. Permission from IEEE must be obtained for all other uses, in any current or future media, including reprinting/republishing this material for advertising or promotional purposes, creating new collective works, for resale or redistribution to servers or lists, or reuse of any copyrighted component of this work in other works.”

This is the author's version of an article that has been published in this journal. Changes were made to this version by the publisher prior to publication.
The final version of record is available at http://dx.doi.org/10.1109/TAP.2021.3060944

Antenna Parameters for On-Body Communications with Wearable and Implantable Antennas

Lukas Berkelmann, *Student Member, IEEE*, Dirk Manteuffel, *Member, IEEE*

***Abstract*—In this contribution, redefined antenna parameters regarding the additional effects occurring with on-body propagation are derived to enable a standardized characterization of on-body antennas. A model for the on-body propagation of arbitrary wearable and implantable antennas using Green's functions based on Norton surface wave theory and the surface equivalence principle is presented which subsequently is used as an on-body near-field to far-field transformation. The defined on-body far-field enables the redefinition of the antenna parameters (gain, effective area and efficiency) for the on-body case. Based thereon, the antennas can be de-embedded from the on-body channel and the on-body link between two antennas can be calculated by an adapted Friis transmission equation similar to free space propagation. It is demonstrated by two examples, one of a hearing aid antenna and another of an antenna of an implantable pacemaker, that the on-body antenna parameters allow for an educated design of the antennas without the necessity of electromagnetic modeling of the entire system.**

***Index Terms*—Wireless body area networks, EM theory, antenna de-embedding, on-body propagation, wearable antennas, implantable antennas.**

I. Introduction

WIRELESS body area networks (WBAN) as part of wearable consumer electronics are long-established. Also, body-attached radio systems are used in many medical applications. Looking at the design methods for such radio systems, only off-body links where just one node of the system is located on the user's body can be treated with the standard free space antenna parameters [1] as they assume a piece-wise free space propagation environment. On-body links with two or more body-attached nodes of a wireless communication system need to be treated differently since the electromagnetic field is partially guided on the tissue boundary and thus propagation differs from the free space case. Also, the antenna's near-field couples to the dissipative tissue making it difficult to de-embed the antenna from the propagation channel and to treat them as separate building blocks. Thus, the standard antenna theory based on the antenna radiation pattern cannot be used to quantify the contribution of the antennas themselves to the link budget along the body surface [2].

Many published approaches for on-body RF communication design circumvent this problem by keeping the antenna embedded in the model. Therefore, they are antenna- and subject-specific (posture, morphology/anatomy and locations of the WBAN nodes). In this manner, standard numerical simulations and path gain measurements treat the whole system as a black box and measured quantities are only available at the outer ports. By observing different antenna positions and body poses, statistical path gain models and channel models can be implemented [3]–[8]. For clearly defined problems, analytical modeling is an option, which is also more suitable for understanding the occurring wave propagation mechanisms in on-body radio systems. E.g. in [9] a comprehensive model for the ear-to-ear propagation is presented. For these on-body to on-body links, it is well understood that in general normally polarized antennas (towards the body surface) present the solution for higher on-body path gains due to the excitation of TM-mode surface waves [2], [9]–[11].

In the area of implantable antennas, previous investigations and models often aim at maximizing the power radiated out of the body (in-body to off-body) [12], [13]. Theoretical models have also been developed for in-body to on-body links, where the antennas are in close distance and displaced to each other mainly in normal direction to the body surface (e.g. for wireless power transfer) [14], [15]. For in-body to on-body links with greater separation between the antennas, surface waves or creeping waves above the body surface play an important role due to the high attenuation in the tissue [16].

As an approach for the antenna characterization for on-body links, in [17] the partial antenna gain with normal polarization towards the body surface is utilized to calculate an on-body radiation pattern for quantifying the creeping wave excitation. However, with the standard free space near-field to far-field (NF-FF) transformation, an undefined part of the body is included in the characterization of the antenna and therefore no reliable results can be obtained. Another approach originating from the creeping wave theory adopted for WBAN [18] is the determination of an on-body gain by measuring the antenna gain above an infinitely large PEC (perfect electric conductor) plane [19]. However, the antenna characterization above PEC has obvious disadvantages because the influence of the tissue on the antenna is not modeled correctly and therefore the input impedance and current distribution on the antenna are not reproduced correctly.

Additionally, as shown in [20], the standard gain calculation of an on-body antenna with reference to an isotropic source reveals a dependency on the distance. Thus, published solutions for the calculation of an on-body gain are still subject-specific and not comparable for different applications. To resolve this, a concept for an on-body antenna pattern is presented in [11], whereas the on-body propagation of wearable antennas is calculated by approximating the body as an infinite tissue half-space. However, the applicability of the model is limited and a certain subject-specificity remains due to the height-dependent

This work was supported by the Deutsche Forschungsgemeinschaft (DFG) under grant MA 4981/11-1.

The authors are with the Institute of Microwave and Wireless Systems, Leibniz University Hannover, Appelstr. 9A, 30167 Hannover, Germany (e-mail: berkelmann@imw.uni-hannover.de, manteuffel@imw.uni-hannover.de)

Copyright (c) 2021 IEEE. Personal use is permitted. For any other purposes, permission must be obtained from the IEEE by emailing pubs-permissions@ieee.org.

This is the author's version of an article that has been published in this journal. Changes were made to this version by the publisher prior to publication.
The final version of record is available at http://dx.doi.org/10.1109/TAP.2021.3060944

TABLE I
STATE-OF-THE-ART: WBAN LINK BUDGET MODELING

Method	Specificity	Applicability
Statistical channel models, e.g. [3]–[8]	specific for antenna and link/channel	wearables and implants
Analytical propagation models, e.g. [2], [9]–[15]	specific for link/channel	wearables and implants
On-body antenna radiation pattern, e.g. [11], [17]	independent of link/channel	wearables

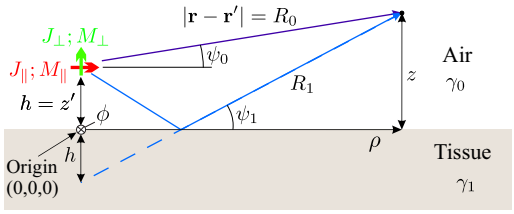

Fig. 1. On-body propagation model based on the Sommerfeld problem.

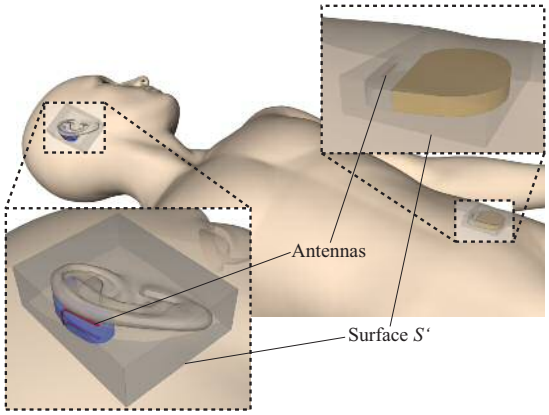

Fig. 2. Example scenarios: a hearing aid antenna at the ear (left) and gastric pacemaker (right) each with the surface S' of the near-field box

normalization to Hertzian dipoles.

As summarized in table I, there are various approaches for WBAN path loss and antenna modeling. However, most of them are specifically adapted to the respective application and/or subject. Only the concept of an on-body antenna radiation pattern potentially allows for a characterization of the antennas independent of the application.

Based thereon, this contribution aims for implementing a complete set of on-body antenna parameters by a reliable and straightforward approach for quantifying the contribution of the antennas themselves to the link budget with on-body communication. In particular, the ability of an antenna to excite surface waves is quantified, which is crucial if WBAN communication takes place over larger distance distances near the tissue-air interface. In section II we develop an on-body propagation model that covers wearable as well as implantable antennas. Based thereon, in section III the on-body far-field is defined. In section IV we define on-body antenna parameters, closely following the definitions in free space [21] to enable good interpretability. Finally, in section V the applicability of the developed methods is proven by two example applications. Additionally, in section VI the limitations for the implementation of our approach are discussed.

II. On-body propagation modeling

With the abstraction of the body surface to an infinitely extended half-space, the structure corresponds to the long-known Sommerfeld half-space problem (ref. Fig. 1). Since the solution of the Sommerfeld integrals cannot be solved in closed-form, there have been many attempts in the literature to derive approximate formulas [22]. The formulation of Norton and especially its extended form by Bannister [23] have been proven to be a suitable approximate solution for the radiation of Hertzian dipoles in the vicinity of a tissue half-space [10], [24], [25]. Following Norton's formulation, the electromagnetic far-field of an antenna above a dissipative ground can be decomposed into quasi-optical components (ref. Fig. 1: direct wave along R_0, reflected wave R_1) and a so-called Norton surface wave component. The latter is particularly important for the link between low profile on-body antennas as it is the only remainder in the limiting case of both the observer and the source located directly on the tissue boundary. Although at first sight the solutions look like a far-field solution with plane wave reflections, the near-field interaction as with on-body antennas is also solved correctly by the spectral decomposition of the spherical waves. In [11] it was shown that on-body fields of arbitrary antennas can be modeled through a decomposition of the antenna's current distribution into small electric dipoles. However, when trying to utilize this method for typical WBAN applications, e.g. for characterizing hearing aid antennas, some difficulties arise. If the antenna is positioned in close proximity to protruding body parts whose near-field influence cannot be approximated well by the half-space, e.g. the pinna, this modeling approach fails to correctly reproduce the radiated fields.

A. Model implementation

To overcome this, in the following we propose using the surface equivalence principle for making the modeling as versatile as possible. Secondly, we derive dyadic Green's functions for the Sommerfeld problem to represent the solution in the most general form.

By means of the surface equivalence theorem, the actual antenna can be replaced by equivalent currents on a closed surface S' enclosing the original sources, as e.g. can be seen in Fig. 2 for two example applications. The choice of the surface is free, it can be above the tissue, intersect with the tissue boundary (as for the hearing aid antenna in Fig. 2) or be inside the tissue (e.g. as for the implantable antenna in Fig. 2). Setting the fields inside the surface to zero, the equivalent electric and magnetic source current densities $\mathbf{J}_\mathrm{s}$ and $\mathbf{M}_\mathrm{s}$ flowing on the surface S' can be calculated as [26]:

$$\mathbf{J}_\mathrm{s}(\mathbf{r}') = \mathbf{n} \times \mathbf{H}(\mathbf{r}'), \tag{1}$$

$$\mathbf{M}_\mathrm{s}(\mathbf{r}') = -\mathbf{n} \times \mathbf{E}(\mathbf{r}'), \tag{2}$$

Copyright (c) 2021 IEEE. Personal use is permitted. For any other purposes, permission must be obtained from the IEEE by emailing pubs-permissions@ieee.org.

This is the author's version of an article that has been published in this journal. Changes were made to this version by the publisher prior to publication.
The final version of record is available at http://dx.doi.org/10.1109/TAP.2021.3060944

where $\mathbf{E}(\mathbf{r}')$ and $\mathbf{H}(\mathbf{r}')$ are the (numerically) calculated near-fields of the antenna on the surface S' and $\mathbf{n}$ is the surface normal pointing outwards the closed surface.

The fields radiated by the structure inside S' can then be calculated by:

$$\mathbf{E}(\mathbf{r}) = \oiint_{S'} \left[\overline{\mathbf{G}}_{\mathrm{J}}^{\mathrm{E}}(\mathbf{r},\mathbf{r}') \cdot \mathbf{J}_{\mathrm{s}}(\mathbf{r}') + \overline{\mathbf{G}}_{\mathrm{M}}^{\mathrm{E}}(\mathbf{r},\mathbf{r}') \cdot \mathbf{M}_{\mathrm{s}}(\mathbf{r}') \right] \mathrm{d}S' \quad (3)$$

$$\mathbf{H}(\mathbf{r}) = \oiint_{S'} \left[\overline{\mathbf{G}}_{\mathrm{J}}^{\mathrm{H}}(\mathbf{r},\mathbf{r}') \cdot \mathbf{J}_{\mathrm{s}}(\mathbf{r}') + \overline{\mathbf{G}}_{\mathrm{M}}^{\mathrm{H}}(\mathbf{r},\mathbf{r}') \cdot \mathbf{M}_{\mathrm{s}}(\mathbf{r}') \right] \mathrm{d}S' \quad (4)$$

where $\overline{\mathbf{G}}_{\mathrm{J}}^{\mathrm{E}}$, $\overline{\mathbf{G}}_{\mathrm{J}}^{\mathrm{H}}$, $\overline{\mathbf{G}}_{\mathrm{J}}^{\mathrm{H}}$ and $\overline{\mathbf{G}}_{\mathrm{M}}^{\mathrm{H}}$ denote the dyadic Green's functions for the on-body case approximated by a tissue half-space which are derived from Bannister's asymptotic solution of the Sommerfeld problem. The derived Green's functions are based on two fundamental solutions with the current flowing either parallel or perpendicular to the boundary, ref. Fig 1, each for magnetic and electric currents. This way the Green's functions for the calculation of the E-field $\overline{\mathbf{G}}_{\mathrm{J}}^{\mathrm{E}}$ and $\overline{\mathbf{G}}_{\mathrm{M}}^{\mathrm{E}}$ in cylindrical coordinates (z-axis normal on tissue surface, ref. Fig. 1) can be written as:

$$\overline{\mathbf{G}}_{\mathrm{J}}^{\mathrm{E}} = \frac{\gamma_0 \eta_0}{4\pi} \begin{pmatrix} G_{\mathrm{J},\rho}^{\mathrm{E},\parallel} & 0 & G_{\mathrm{J},\rho}^{\mathrm{E},\perp} \\ 0 & G_{\mathrm{J},\phi}^{\mathrm{E},\parallel} & 0 \\ G_{\mathrm{J,z}}^{\mathrm{E},\parallel} & 0 & G_{\mathrm{J,z}}^{\mathrm{E},\perp} \end{pmatrix}, \quad (5)$$

$$\overline{\mathbf{G}}_{\mathrm{M}}^{\mathrm{E}} = \frac{\gamma_0}{4\pi} \begin{pmatrix} 0 & G_{\mathrm{M},\rho}^{\mathrm{E},\parallel} & 0 \\ G_{\mathrm{M},\phi}^{\mathrm{E},\parallel} & 0 & G_{\mathrm{M},\phi}^{\mathrm{E},\perp} \\ 0 & G_{\mathrm{M,z}}^{\mathrm{E},\parallel} & 0 \end{pmatrix}, \quad (6)$$

where $G^{\{\parallel,\perp\}}$ with the unit m^{-1} are the Green's functions for the E-field derived from the solution of current elements in parallel ($\parallel$) or the normal ($\perp$) orientation towards the tissue surface.[1] The magnetic field's Green's function can be derived similarly. Other than in free space, the Green's functions not only depend on the distance $\mathbf{r} - \mathbf{r}'$ between source and observation point, but also directly on the height h of the source above the tissue boundary (in the selected coordinate system, ref. Fig 1, $h = z'$). To calculate the radiated field in air for the subsurface-case (implantable antenna, $h < 0$), the necessary Green's functions can be obtained from $G(h = 0) \cdot e^{\gamma_1 h}$, with the complex propagation constant γ_1 of the tissue [23]. Additionally, the term $G_{\mathrm{J,z}}^{\mathrm{E},\perp}$ gets multiplied with $\gamma_0^2 \gamma_1^{-2}$ for $h < 0$ to satisfy the boundary condition.

The only limitation of the utilized asymptotic solutions [23] for deriving the Green's functions G is a high contrast between the materials, respectively an index of refraction of the tissue-air boundary of $|n^2| > 10$. As shown in [24], this condition is maintained for most tissues across all WBAN frequency bands of interest. However, for conciseness we concentrate on the evaluation of the method in the 2.4 GHz ISM band. Therefore, the utilized single-layer tissue model provides a good approximation for the propagation behavior [10]. In general, the approach can also be extended to a multilayered tissue model [27].

[1]The individual Green's function terms are listed in Appendix B

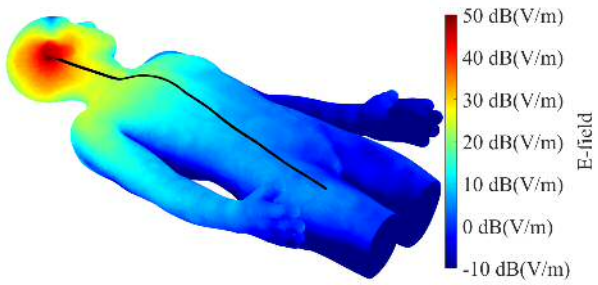

Fig. 3. E-field distribution at constant height of 10 mm above the phantom surface and the evaluated path

Besides the generalization and inclusion of implantable antennas, the new approach has the advantage that the modeling can be implemented more streamlined for numerical input data. Taking the antenna's discretized on-body near-field as a basis (same as with the standard free NF-FF transformation), the integrals in (5) and (6) can be written as a sum in which the discrete surface currents $[J_{\mathrm{s}}] = \mathrm{A/m}$ respectively $[M_{\mathrm{s}}] = \mathrm{V/m}$ multiplied with the corresponding mesh cells surface area $[\Delta S'] = \mathrm{m}^2$ correspond with the dipole moments $[p] = \mathrm{Am}$ and $[m] = \mathrm{Vm}$ in the derivation of the Sommerfeld problem solution [23]. [2]

B. Example application

To prove the applicability of our approach, we used an example of a simplified hearing aid model (ref. Fig. 2) which was modeled consisting of ABS plastic (permittivity $\varepsilon_{\mathrm{r}} = 2.7$, loss tangent $\tan\delta = 0.005$). The antenna is designed as a conformal half-wave dipole on the hearing aid housing at $f = 2.45$ GHz. For the modeling we utilized the near-field on the surface S' of the antenna including the pinna as depicted in Fig. 2. This way, the pinna is basically treated as part of the antenna. As can be seen from the results in Fig. 4a, calculated above a flat phantom (equivalent to the infinite half-space of the analytical model), the new modeling approach is proven to be precise. The deviation of the E-field is less than 1 dB in the far-field of the antenna. Secondly, we evaluated the E-Field captured on a realistic path along the body at a constant height of 10 mm above the phantom surface. The results for the E-field on this surface and the evaluated path are depicted in Fig. 3. In Fig. 4b the fields along the path obtained from the numerical simulation are compared to the results calculated with our modeling approach. As can be seen, the model reveals a deviation of less than 3 dB from the numerical results along nearly the whole evaluated path.

III. On-body far-field

As shown in the previous section, the proposed modeling approach enables the modeling of the on-body fields of wearable and implantable antennas. However, only a small part

[2]The original solution for magnetic dipoles in [23] is based on the current loop representation $[m_l] = \mathrm{Am}^2$ which can be converted to magnetic current dipoles $[m] = \mathrm{Vm}$ with $m = j\omega\mu_0 m_l$. [26]

Copyright (c) 2021 IEEE. Personal use is permitted. For any other purposes, permission must be obtained from the IEEE by emailing pubs-permissions@ieee.org.

This is the author's version of an article that has been published in this journal. Changes were made to this version by the publisher prior to publication.
The final version of record is available at http://dx.doi.org/10.1109/TAP.2021.3060944

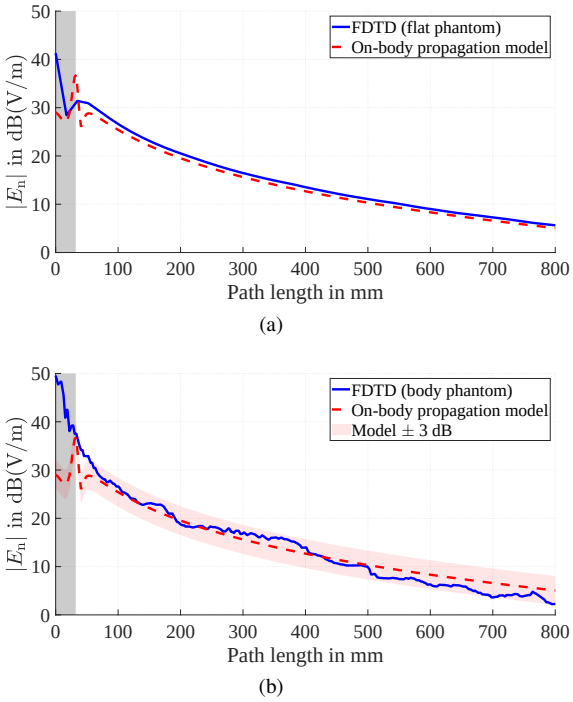

Fig. 4. Verification of the implemented method by comparison of the calculated E-field to numerical results: (a) Ideal flat tissue halfspace, (b) Realistic path along body phantom (ref. Fig. 3). The section inside surface S' is marked with a grey background. Only the normal component of the E-field with respect to the body surface was evaluated, as this is the dominating component (in our example by more than 10 dB) close to the tissue interface.

of the possible applications include paths that are sufficiently flat to be directly modeled through the Sommerfeld problem. Besides that, it is desirable to evaluate an on-body antenna completely independent of the application scenario, i.e. de-embedded from the propagation channel. In this section, we evaluate how to define the on-body far-field with the half-space approximation which enables the definition of adapted on-body antenna parameters. Subsequently, we discuss its applicability also for the propagation along curved paths.

For radiation in free space, the far-field region is defined by the consideration that the radiated waves can locally be represented by a plane wave. In the free space far-field, the power density decreases quadratically with increasing distance from the radiator for any antenna. Thus, the antenna gain defined as a relative indication of the radiation properties of the antenna compared with those of a reference is independent of the distance from the radiator.

The case of an antenna above or inside a dissipative tissue is more complex due to the interference of the different wave components (direct, reflected and Norton surface wave). Additionally, waves propagating along the boundary are attenuated by losses in the tissue. Thus, the standard antenna gain calculation for on-body antennas reveals a dependency on the distance.

To resolve this, a different approach has to be made for defining an antenna metric for on-body links. For quantifying the ability of exciting waves along the body surface, it seems reasonable to only characterize the antenna's two-dimensional angle-dependent radiation parallel to the body surface. The

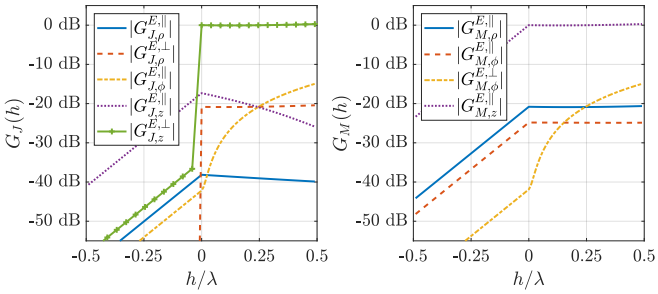

Fig. 5. Normalized magnitude of the Green's functions of equation 5 and 6 at $\rho = 10\lambda$ and $z = \lambda/4$ as a function of the height h

inconsistency because of the additional attenuation due to losses in the tissue can be dealt with an adapted normalization (replacement of the lossless isotropic source). Therefore, in the on-body far-field this attenuation needs to be equal for all antennas to be considered. Additionally, amplitude and phase deviation across the wavefront near the tissue boundary must be negligible to recreate the local plane wave criteria.

In the following, we evaluate under which circumstances these requirements can be met for low profile antennas (standard requirement for on-body antennas) close above or below the body surface. Due to the boundary condition at the conductive tissue, the magnitude of the different Green's functions G near the boundary depends largely on their corresponding polarization. In Fig. 5 we depict the normalized magnitude of the Green's functions for the E-field as a function of the antenna height h. As can be seen, for low heights the terms $G^{\mathrm{E},\perp}_{\mathrm{J,z}}$ and $G^{\mathrm{E},\parallel}_{\mathrm{M,z}}$ exceed all others by about 20 dB, which correlates with the prior knowledge that antennas polarized normally to the body surface provide a higher on-body path gain [2], [9]–[11]. Thus, in the following we concentrate on these components for the evaluation of the on-body far-field.

Far from the antenna with $|\gamma_0 R_1| >> 1$ these two dominating terms can be indicated in a simplified manner as [23]:

$$G^{\mathrm{E},\perp}_{\mathrm{J,z}} = \cos^2(\psi_0)\frac{e^{-\gamma_0 R_0}}{R_0} + \Gamma_\perp \cos^2(\psi_1)\frac{e^{-\gamma_0 R_1}}{R_1} + (1-\Gamma_\perp)F(w)\cos^2(\psi_1)\frac{e^{-\gamma_0 R_1}}{R_1}, \tag{7}$$

$$G^{\mathrm{E},\parallel}_{\mathrm{M,z}} = \cos(\psi_0)\frac{e^{-\gamma_0 R_0}}{R_0} + \Gamma_\perp \cos(\psi_1)\frac{e^{-\gamma_0 R_1}}{R_1} + (1-\Gamma_\perp)F(w)\cos(\psi_1)\frac{e^{-\gamma_0 R_1}}{R_1}, \tag{8}$$

with R_0, R_1, ψ_0 and ψ_1 the lengths and elevation angles of direct and reflected paths from the source currents (ref. Fig. 1). The structure of the equations is equivalent to the well-known Norton surface wave model and can therefore be translated into the components of a direct wave (1st term), a reflected wave (2nd term) and the Norton surface wave (3rd term). $F(w)$ is the Sommerfeld surface wave attenuation factor with the numerical distance w which depends in a rather complex way on geometry and material parameters. By restricting the evaluation for the on-body case to low

Copyright (c) 2021 IEEE. Personal use is permitted. For any other purposes, permission must be obtained from the IEEE by emailing pubs-permissions@ieee.org.

This is the author's version of an article that has been published in this journal. Changes were made to this version by the publisher prior to publication.
The final version of record is available at http://dx.doi.org/10.1109/TAP.2021.3060944

heights and correspondingly small angles ψ, the specular reflection coefficient for perpendicular-polarized waves $\Gamma_\perp$ can be approximated as:

$$\Gamma_\perp = \frac{\sin(\psi_1) - \Delta_m}{\sin(\psi_1) + \Delta_m} \approx \frac{\psi_1 - \Delta_m}{\psi_1 + \Delta_m}, \tag{9}$$

with $\Delta_m = \frac{\gamma_0}{\gamma_1}$. Further approximations can be made as follows:

$$\cos(\psi_0) \approx \cos(\psi_1) \approx 1; \qquad \frac{1}{R_0} \approx \frac{1}{R_1} \approx \frac{1}{\rho}.$$

Since with the approximations made, both dominating Green's function terms differ only in the exponent of the cosine terms, they converge to each other for low heights. Thus, low-profile antennas can be expected to produce similar on-body field distributions in the far-field close to the tissue boundary.

In the case of pure surface to surface propagation with $h = 0$ and $z = 0$, corresponding to an angle of $\Psi_1 = 0°$, the Green's functions consist only of the Norton surface wave term. This is because the reflection coefficient as with total internal reflection (TIR) becomes $\Gamma_\perp = -1$ and direct wave and reflected wave cancel each other out. Also, the Sommerfeld attenuation factor $F(w)$ becomes a function only depending on the radial distance ρ as stated in [23]:

$$F(\rho) = 1 - j\sqrt{\pi K \rho} \cdot w_{\mathrm{F}}(-\sqrt{K\rho}), \tag{10}$$

with $w_{\mathrm{F}}(x)$ the Faddeeva function and $K = -0.5\gamma_0\Delta_{\mathrm{m}}^2$.

A. On-body far-field distance

To define the on-body far-field, we derive limits for the region where the Green's functions can be approximated by the Norton surface wave term. On closer analysis, this condition can be translated into two requirements. Firstly, the phase difference $\Delta\phi_{\mathrm{r}}$ between direct and reflected waves must be negligible:

$$\Delta\phi_{\mathrm{r}} = |\gamma_0|\,(R_0 - R_1) \approx 0. \tag{11}$$

An estimation can be made by restricting the phase difference to $\Delta\phi_{\mathrm{r}} \leq \pi/8$.[3] With the approximation of parallel paths R_0 and R_1 this leads to a far-field distance of:

$$\rho \geq \sqrt{\left(\frac{16hz\,|\gamma_0|}{\pi}\right)^2 - h^2}. \tag{12}$$

Secondly, the reflection coefficient $\Gamma_\perp$ needs to be negative such that direct and reflected wave interfere destructively. According to (9), the coefficient $\Gamma_\perp$ can be calculated from the angle ψ_1 which varies with the distance ρ and Δ_{m} which is a constant complex number depending on the material parameters of the tissue. By analyzing its behavior as a function of the distance ρ, it can be found that:

$$\arg\{\Gamma_\perp\}(\rho \to 0) \approx 0, \qquad \arg\{\Gamma_\perp\}(\rho \to \infty) = \pi.$$

The distance where $\arg\{\Gamma_\perp\} \approx \pi/2$ can be determined by $\psi_1 = \mathrm{Re}\{\Delta_m\}$. Under the assumption of $\left(\frac{\sigma}{\omega\varepsilon_0}\right)^2 \ll 1$ and

[3]Same limit was chosen for the definition of the widely accepted Fraunhofer far-field distance

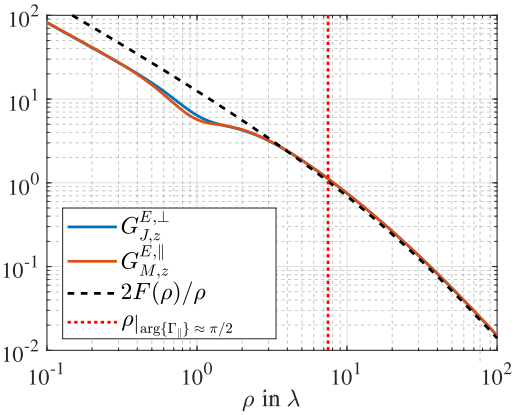

Fig. 6. Green's functions of equation 7 and 8 for $z = h = \lambda/2$ in comparison to the surface wave attenuation factor $F(\rho)$ and the corresponding far-field distance of Equation 13

$\psi_1 \approx \frac{z+h}{\rho}$, this leads to a second restriction for the far-field distance:

$$\rho \geq \frac{z+h}{|\Delta_m|^2\sqrt{\varepsilon_{r,1}}}\,. \tag{13}$$

Both conditions must be satisfied to ensure the field's approximation by the surface wave term only, thus fulfilling the on-body far-field criteria. As can be seen, both depend on the transmitter's height h as well as on the receiver's height z. For extended antenna structures, the distance of the highest point above the tissue surface needs to be used. If an antenna's dimensions parallel to the tissue interface are significantly larger than its height, the standard Fraunhofer distance $d \geq \frac{2D^2}{\lambda}$ [21] can be used to ensure a sufficient plane wave approximation accounting also for superimposing wave components through parallel displaced origins. In the case of implantable antennas, the on-body far-field distance is significantly reduced as in the calculation the transmitter's height can be set to $h = 0$ (fields for $h < 0$ can be modeled through $G(h = 0)$ and an additional constant factor, ref. Sec. II-A). Assuming muscle tissue at $f = 2.4\,\mathrm{GHz}$, the second condition from (13) gives greater distances and thus can be calculated solely. In Fig. 6 the dominating Green's functions $G_{\mathrm{J,z}}^{\mathrm{E},\perp}$ and $G_{\mathrm{M,z}}^{\mathrm{E},\parallel}$ are depicted exemplary, calculated at the maximum height evaluated of $z = h = \lambda/2$. Here, the far-field distance according to (13) gives a value of $\rho \geq 7.5\lambda$. As required, at this range the trajectories of both Green's functions have sufficiently converged into the surface wave attenuation term $F(\rho)$.

Since, as mentioned before only low-profile antennas are considered, the plane wave approximation in the defined on-body far-field is only marginally interfered by the waves amplitude deviation depending on the height above the tissue surface. In the example with a maximum transmitter height of $h = 0.5\lambda$, the deviation at the far-field distance (ref. Fig. 6) over the range of $0 \leq z \leq 0.5\lambda$ is approximately 0.1 dB and is therefore negligible.

Copyright (c) 2021 IEEE. Personal use is permitted. For any other purposes, permission must be obtained from the IEEE by emailing pubs-permissions@ieee.org.

This is the author's version of an article that has been published in this journal. Changes were made to this version by the publisher prior to publication.
The final version of record is available at http://dx.doi.org/10.1109/TAP.2021.3060944

B. Influence of the body's curvature

Up to this point, on-body propagation was modeled purely with the approximation of the body as an infinitely extended half-space. However, in real applications curvatures also play an important role. Fortunately, both problems are closely related as shown by Wait in [27]. For the half-space problem with pure surface wave propagation ($h = z = 0$), which we have shown is also a valid approximation in the on-body far-field, Wait rewrites the solution for the normally polarized E-field as:

$$E^{\perp} = E_0 F(\rho), \tag{14}$$

where $F(\rho)$ is the aforementioned Sommerfeld attenuation factor. The term E_0 is denoted as a reference field which corresponds to fields excited above a PEC plane. This term can also be found in Wait's notation for the creeping wave propagation around a cylindrical curvature [27]:

$$E^{\perp} = E_0 W(x, q). \tag{15}$$

Here, $W(x, q)$ represents the attenuation function for the creeping wave problem which depends on the x as a normalized range parameter and q accounting for the curvature's radius. Thus, the properties of the excitation, i.e. the antenna, are quantified with E_0 in both cases. This was already utilized in [18] to model on-body propagation along curved body parts. However, as mentioned before, modeling the antenna above a PEC has obvious disadvantages because the influence of the tissue on the antenna is not modeled correctly and therefore the input impedance and current distribution on the antenna are not reproduced correctly. If on the other hand the excitation is quantified over a tissue half-space as we have shown, this problem can be omitted. After normalization by the attenuation term $F(\rho)$, as derived in the following, the application of the on-body antenna parameters calculated in the case of a flat tissue half-space is equally possible for propagation channels with curved surfaces.

IV. On-body antenna parameters

Based on the defined on-body far-field, an on-body radiation pattern can be defined. As mentioned before, to quantify an antenna's ability of exciting waves traveling along the body surface, a two-dimensional angle-dependent measure for the radiation parallel to the body surface is sufficient. Thus, based on the definition in free space (FS), the antenna's directivity can be adapted for on-body (B) propagation to:

$$D_{\mathrm{FS}}(\theta, \phi) = \frac{U(\theta, \phi)}{\overline{U}} \;\rightarrow\; D_{\mathrm{B}}(\phi) = \frac{U^{\perp}(\phi)}{\overline{U^{\perp}}}. \tag{16}$$

Here $U^{\perp}(\phi)$ is the radiation intensity corresponding to the normal polarization only, since it dominates close to the tissue boundary in the far-field, as e.g. can be seen from Fig. 5. Because in the on-body far-field the amplitude ratio of the associated Green's functions for $E^{\perp}$ and $H^{\parallel}$ also is $\eta_0 = \mu_0 \varepsilon_0$, the radiation intensity can be calculated as:

$$U^{\perp}(\phi) = \rho^2 \frac{1}{2} E^{\perp}(\phi) H^{\parallel}(\phi) = \frac{\rho^2 {E^{\perp}}^2(\phi)}{2\eta_0}. \tag{17}$$

To quantify the surface wave radiation solely, the mean intensity $\overline{U^{\perp}}$ for the directivity is only determined over ϕ in the plane parallel to the body surface as:

$$\overline{U^{\perp}} = \frac{1}{2\pi} \oint_{2\pi} U^{\perp}(\phi) \mathrm{d}\phi. \tag{18}$$

Other than in free space, the radiation intensity $U^{\perp}$ is dependent on the distance because of the additional attenuation of the surface wave traveling along the tissue boundary. For the on-body far-field, this surface wave attenuation can be quantified by $2|F(\rho)|$ as shown in the previous section. Thus, following the derivation in free space, the on-body antenna gain can be defined as:

$$G_{\mathrm{FS}}(\theta, \phi) = \frac{U(\theta, \phi)}{P_{\mathrm{in}}/4\pi} \rightarrow G_{\mathrm{B}}(\phi) = \frac{U^{\perp}(\phi)}{P_{\mathrm{in}} |F(\rho)|^2 / \pi}. \tag{19}$$

with P_{in} the power accepted at the antenna port. The constant ratio between on-body gain and directivity also gives an adapted definition of the antenna efficiency:

$$e_{\mathrm{B}} = \frac{G_{\mathrm{B}}}{D_{\mathrm{B}}} = \frac{\pi \overline{U^{\perp}}}{|F(\rho)|^2 P_{\mathrm{in}}}. \tag{20}$$

This measure quantifies the ratio between power accepted at the port and power radiated in form of the surface wave. The relation between the on-body gain and the effective area (aperture) can be calculated by the same procedure as in free space to[4]:

$$A_{\mathrm{e,B}} = \frac{\lambda^2}{4\pi} G_{\mathrm{B}}. \tag{21}$$

Finally, the Friis transmission equation for on-body propagation can be reassembled to:

$$\frac{P_{\mathrm{r}}}{P_{\mathrm{t}}} = \underbrace{\left(\frac{\lambda L_{\mathrm{SW}}}{4\pi\rho} \right)^2}_{F_{\mathrm{B}}} G_{\mathrm{B,t}} G_{\mathrm{B,r}}. \tag{22}$$

Here L_{SW} describes the surface wave attenuation, which depends on the body curvature along the path evaluated. For sufficiently flat sections of the path, it can be calculated as $L_{\mathrm{SW}} = 2F(\rho)$, and for curved path sections the term can be determined by $L_{\mathrm{SW}} = 2W(x, q)$ (ref. Sec. III-B).

V. Example application of the developed methods

To illustrate the possibilities of the described methods, we investigate two example problems, one for a wearable and one for an implantable antenna. As mentioned before, we concentrate on the evaluation of the methods in the 2.4 GHz ISM band. Simple dipole antennas were used since the focus is not on the antenna design but on the verification of the developed methods. The utilized body phantom in both cases was modeled assuming homogeneous muscle tissue ($\varepsilon_r = 52.7$, $\sigma = 1.74\,\mathrm{S/m}$), which is a sufficient approximation at the considered frequency [10]. Two different paths were evaluated, as can be seen in Fig. 7. Path 1 along the torso was chosen to be relatively flat. In contrast, path 2 around the torso contains curved sections and has no line-of-sight.

[4]The proof based on a Hertzian dipole can be found in Appendix A.

Copyright (c) 2021 IEEE. Personal use is permitted. For any other purposes, permission must be obtained from the IEEE by emailing pubs-permissions@ieee.org.

This is the author's version of an article that has been published in this journal. Changes were made to this version by the publisher prior to publication.
The final version of record is available at http://dx.doi.org/10.1109/TAP.2021.3060944

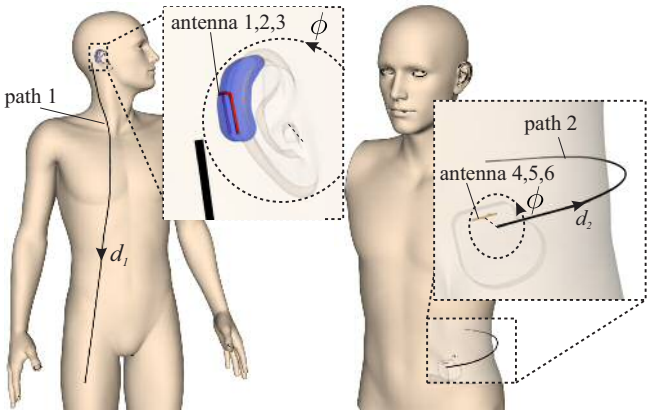

Fig. 7. Evaluated example applications of a hearing aid antenna and a gastric pacemaker.

The described methods for the calculation of the defined on-body antenna parameters were implemented for the examples as follows:

1) Numerical (FDTD) calculation of the antenna's near-field on the surface S' in presence of the body phantom as depicted in Fig 2,
2) On-body NF-FF transformation using the on-body propagation model as described in Sec. II-A and the derived Green's functions in Appendix B,
3) Calculation of the antenna parameters as described in Sec. IV.

A. Radiation of wearable antenna along flat path

As an example of a wearable antenna, we continue with the hearing aid antenna design as shown in Fig. 7. To compare the effects of different antenna patterns along path 1, the conformal dipole is positioned on the housing in three different configurations (antenna 1-3), as can be seen in Fig. 8.

Fig. 9a depicts the calculated on-body antenna gain according to (19) for all three antenna configurations. The minimum on-body far-field distance is calculated by (13) for a maximum height $z = 17\,\mathrm{mm}$ to $\rho_{\min} \approx 200\,\mathrm{mm}$ for a receiver height of $z = 10\,\mathrm{mm}$.

In the next step, we evaluated the radiated fields of all three hearing aid antenna configurations (ref. Fig. 8) along path 1 to characterize e.g. the wireless link of a hearing aid to a smartphone. In Fig. 9b the path gain (PG) of the antennas calculated with the adapted Friis transmission equation (22) is compared to FDTD calculated data of the actual geometry as reference. Therefore, the surface wave attenuation was calculated assuming a flat body surface. As can be seen, the overall trend in the path gain is sufficiently modeled, even though locally noticeable deviations occur due to geometric irregularities compared to the ideally simplified flat body surface. Furthermore, the path gain for all three antennas deviates with the same pattern from the analytical model and the difference between the different antennas seems constant. In order to assess this better, in Fig. 9c the path gain is normalized to that of antenna 1. Here it can be seen that the difference in the established on-body gain in the path direction (ref. Fig. 9a) precisely predicts the difference between the different antennas considered. Beyond the minimum far-field distance $\rho_{\min}$, the relative path gain predicted from the on-body gain deviates by less than $1\,\mathrm{dB}$ from the numerically calculated reference.

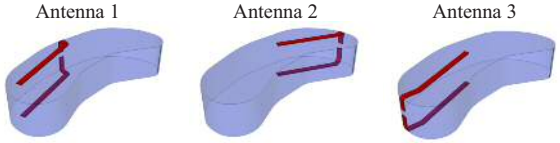

Fig. 8. Conformal dipole on hearing aid housing in three different configurations

B. Radiation of implantable antenna along curved path

As for the example of an implantable antenna, we evaluate the application of a gastric pacemaker, which is depicted in Fig 7. We investigated the on-body radiation along path 2 around the torso which has a significant curvature. The antenna consists of a half-wave dipole encapsulated by a $1.3\,\mathrm{mm}$ thick substrate ($\varepsilon_\mathrm{r} = 10.2$) implanted in a depth of $10\,\mathrm{mm}$. For simplicity, no additional peripherals of the implant were modeled in the simulation. The minimum on-body far-field distance in this case is $\rho_{\min} \approx 75\,\mathrm{mm}$. To compare the propagation for different gain values in this case, the antenna was rotated in the three different angles ($\Delta\phi = 30°$) in the plane parallel to the tissue surface. Consequently, as depicted in Fig. 10a, the radiation pattern quantified in form of the on-body gain varies in direction of the evaluated path 2 by $\Delta G_{\mathrm{B},5} = 3.3\,\mathrm{dB}$ for antenna 5 and $\Delta G_{\mathrm{B},6} = 9.8\,\mathrm{dB}$ for antenna 6, provided that antenna 4 is used as reference. Looking at the path gain along path 2 in Fig. 10b, one can see that it partially declines more rapidly than for the flat case because of the body curvature. A better estimate using the adapted on-body Friis equation (22) can be made by calculating the surface wave attenuation L_{SW} from the first creeping wave mode assuming a cylindrical curvature with a radius of $140\,\mathrm{mm}$, as proposed in [18]. The deviation of the simple model from the numerical data of the realistic geometry is still significantly higher in this case. However, all three antennas still show the same pattern in the path gain. Thus, by comparing the relative path gain with antenna 4 as reference as depicted in Fig. 10c, again the difference in the on-body gain precisely predicts the path gain difference of the antennas in the numerically calculated realistic model. On closer evaluation, in the numerically calculated data, the influence of multi-path propagation becomes apparent (especially for antenna 6 which has the lowest gain along the direct path) which is not accounted for in the utilized analytical model. In respect thereof, just like in free space, the on-body gain defined in this paper can also be embedded in more advanced path loss models accounting for multi-path propagation and non-cylindrical curved sections as e.g. proposed in [9].

Copyright (c) 2021 IEEE. Personal use is permitted. For any other purposes, permission must be obtained from the IEEE by emailing pubs-permissions@ieee.org.

This is the author's version of an article that has been published in this journal. Changes were made to this version by the publisher prior to publication.
The final version of record is available at http://dx.doi.org/10.1109/TAP.2021.3060944

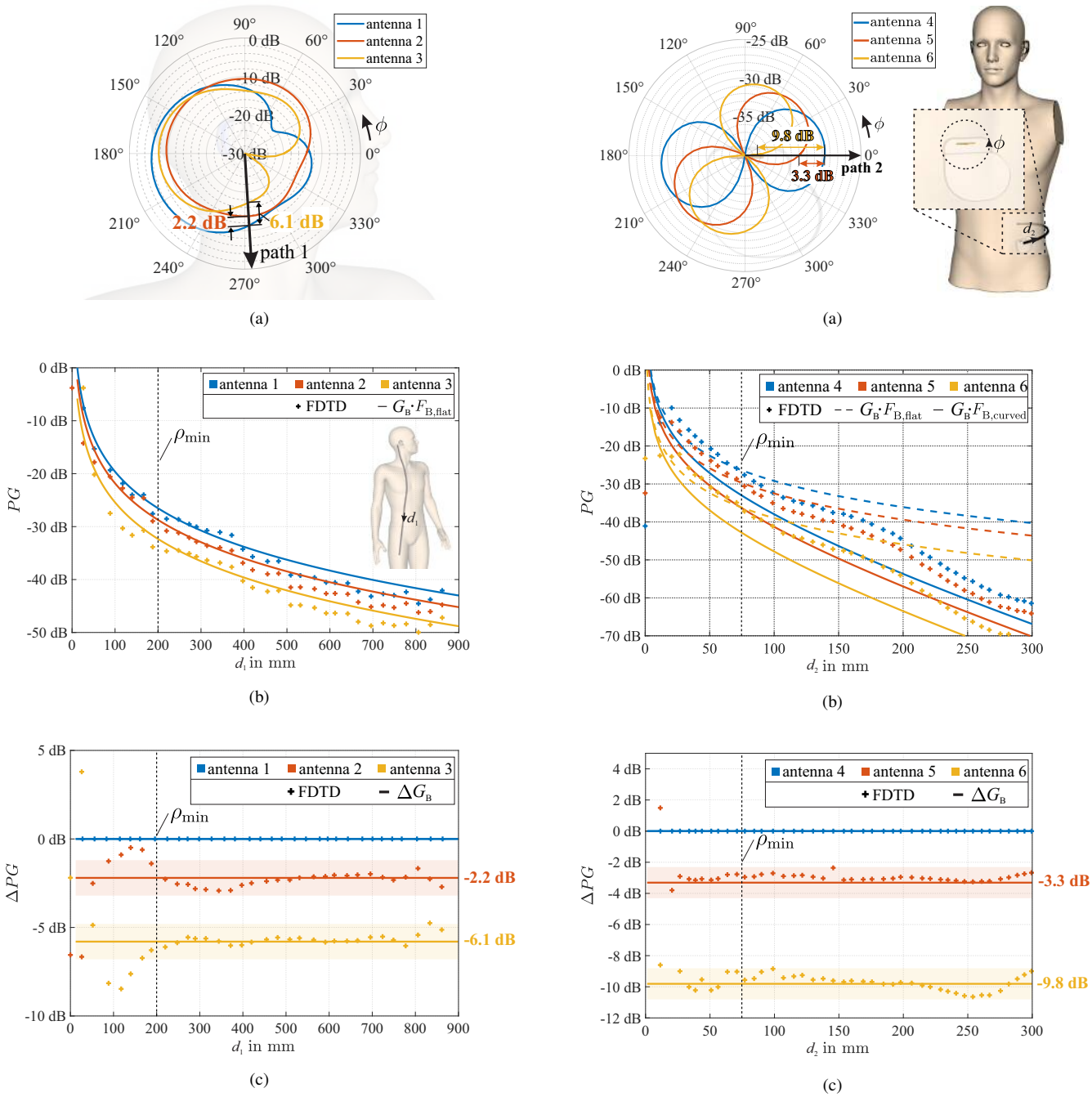

Fig. 9. Antennas 1-3: (a) on-body gain G_B; (b) on-body path gain at a height of 10 mm above the tissue surface; (c) path gain difference with antenna 1 as reference. Shaded areas mark the deviation limited to ± 1 dB

Fig. 10. Antennas 4-6: (a) on-body gain G_B; (b) on-body path gain at a height of 10 mm above the tissue surface; (c) path gain difference with antenna 4 as reference. Shaded areas mark the deviation limited to ± 1 dB

C. On-body efficiency

For some applications, no specific radiation direction can be emphasized. In this case, with standard free space antenna design, the antenna's radiation efficiency is optimized, as the ratio between power delivered to the antenna and power radiated from the antenna. For on-body links, as discussed before, the excitation of surface waves is most important. This is why we also defined an adapted antenna efficiency according to (20), which quantifies the ratio between the power accepted by the antenna and the power radiated in form of the surface wave. Looking back at the example of the hearing aid antennas of Sec. V-A, the corresponding on-body efficiencies can be found in table II. As can be seen, antenna 1 not only has the highest gain in the direction of the evaluated path but also the highest on-body efficiency, so it can be expected on average to result in the highest on-body path gain (among many different paths).

TABLE II
ON-BODY ANTENNA EFFICIENCY RESULTS

	antenna 1	antenna 2	antenna 3
e_B	10.8%	7.0%	6.1%

Copyright (c) 2021 IEEE. Personal use is permitted. For any other purposes, permission must be obtained from the IEEE by emailing pubs-permissions@ieee.org.

This is the author's version of an article that has been published in this journal. Changes were made to this version by the publisher prior to publication.
The final version of record is available at http://dx.doi.org/10.1109/TAP.2021.3060944

VI. Limitations of the Approach

In our derivations, different assumptions and simplifications of the complex antenna environment in presence of the body were made. We discuss the range of validity of these assumptions and outline limitations of the presented theory in the following.

A. Dominant propagation mechanism

The presented theory can be applied for propagation paths which dominantly rely on surface waves or creeping waves. This is very often the case in WBAN applications and covers especially those cases where the performance needs to be optimized. Therefore, as derived in Sec. III the electrical height h of the antenna should be small, which in the usually used WBAN frequency bands (low GHz range) is in accordance with the standard low profile requirements for portability. E.g. the maximum height under consideration in our evaluation of $h = 0.5\lambda$ equals approximately $6\,\mathrm{cm}$ at $2.4\,\mathrm{GHz}$, which is far beyond commonly accepted antenna dimensions. On the other hand, no limits need to be set for the implantation depth of in-body antennas, since the corresponding Green's functions are assembled from the case with $h = 0$, ref. Sec. II-A. However, the significance of the surface wave in relation to the competing propagation path directly through tissue should be checked. In our example with the implanted gastric pacemaker and propagation around the torso, ref. Fig. 7, the direct path through the torso has a length of $l \approx 170\,\mathrm{mm}$. The corresponding attenuation can be estimated by $L_{\mathrm{in-body}} \approx -66\,\mathrm{dB}$.[5] Compared to the attenuation of the creeping wave of $L_{\mathrm{SW}} \approx -33\,\mathrm{dB}$[6] it is obvious, that as required the surface wave is the dominant propagation mechanism in our example.

B. Tissue modeling

For conciseness, the Green's functions as proposed before were derived assuming a single homogeneous tissue model. This is a reasonable simplification in regard of the propagation properties at sufficiently low frequencies (approximate range below $3\,\mathrm{GHz}$ [10]). Due to the decreasing skin depth for higher frequencies, the Green's functions must be adapted for considering a multilayered tissue model, for the necessary adjustments ref. [10], [27]. In certain cases, additional effects such as trapped surface waves can occur due to the multiple boundary layers, which are not covered by our model. However, at millimeter wave frequencies again the simplified assumption of a homogeneous half-space can be made. In this case the dielectric properties of the skin must be considered, as the penetration depth becomes so small that underlying tissues can be neglected [28]. Apart from the influence of the tissue modeling on propagation, especially with implantable antennas the antenna properties are strongly impaired by surrounding tissue [12]. A homogeneous or layered tissue representation, as also assumed by many other in-body antenna theories [12]–[15], is to be seen critically here. By including parts of the surrounding tissue within the reference surface S', ref. Fig 2, into to the antenna properties, inhomogeneous tissues surrounding the antenna can be considered with our theory. For conciseness a detailed analysis on this is left out here.

[5] Assuming homogeneous tissue: $L_{\mathrm{in-body}} = e^{-\mathrm{Re}\{\gamma_1\}l}$.

[6] $L_{\mathrm{SW}} = 2W$ [18] with radius $a = 140\,\mathrm{mm}$ and length $d = 395\,\mathrm{mm}$.

C. Body curvature

As proposed in Sec. II, the on-body NF-FF transformation is based on the assumption of tissue half-space. Therefore, the body surface in direct vicinity of the antenna must be sufficiently flat, such that the near-field on surface S' (ref. Fig. 2) is reproduced correctly. However, with our approach protruding body parts, e.g. the ear, can be taken into account as part of the antenna. To check the validity of this assumption, in the example with the hearing aid antennas, ref. Fig 7, we compared the difference in the on-body Gain G_{B} once calculated with the near-field simulated in presence of the head and once with antenna and ear placed above a flat tissue layer. The maximum deviation was found with antenna 1 with a gain difference of $0.4\,\mathrm{dB}$, which still seems acceptable and proves the validity in this case. Additionally, the channel modeling is also limited in regard of the body curvature. The modeling based on the creeping wave theory reduced to the first mode as applied in the examples requires a curvature perimeter $p \gg \lambda$, which at $2.4\,\mathrm{GHz}$ is sufficient for modeling the shape of an adult head [18]. The more sophisticated approach of a geometrical theory of diffraction model by Kammersgaard et. al. is rated similarly with a validity for radii down to $q > 0.5\lambda$ [29].

VII. Conclusion

We developed a method that enables a universal characterization of the on-body radiation characteristics of wearable and implantable antennas. The derivation of the on-body antenna parameters is linked as closely as possible to the established definition in free space to ensure good interpretability. Through the normalization of the attenuation due to losses in the tissue, the derived gain and antenna efficiency are constant in the on-body far-field. This makes the characterization subject-independent and enables good comparability. The simple geometry of the utilized body phantom in the derivation of the on-body antenna parameters is beneficial for a standardized numerical evaluation and especially for the repeatability of future measurements. For cases limited to only one significant propagation path, as with the examples presented, the path gain difference between different antennas can be precisely predicted from the on-body gain. To model multi-path propagation, the antennas can be embedded in more advanced models while maintaining the advantages of comparability. Since the underlying principles of propagation along the dissipative body surface are similar even with curved body contours, the derived antenna parameters are also valid in this case as shown in the examples.

Copyright (c) 2021 IEEE. Personal use is permitted. For any other purposes, permission must be obtained from the IEEE by emailing pubs-permissions@ieee.org.

This is the author's version of an article that has been published in this journal. Changes were made to this version by the publisher prior to publication.
The final version of record is available at http://dx.doi.org/10.1109/TAP.2021.3060944

APPENDIX A
DERIVATION OF THE ON-BODY ANTENNA EFFECTIVE AREA IN RELATION TO THE ON-BODY GAIN

The derivation is based on the procedure for free space according to [21] where it is shown that the effective area A_e of the isotropic antenna can be calculated from the ratio between gain and effective area of any other antenna. In the following, we prove at the example of a normal Hertzian dipole above the tissue half-space that this relationship stays the same for the newly defined on-body gain according to (21).

Under the condition of maximum power transfer (conjugate matching) and a lossless antenna structure the effective area of a short dipole antenna can be calculated as:

$$A_\mathrm{e} = \frac{(E_\mathrm{i} \cdot l)^2}{8 W_\mathrm{i} R_\mathrm{r}}, \tag{23}$$

where E_i and W_i are the electric field strength and power density of the incoming wave. R_r is the antenna's radiation resistance, which depends on the dipole's length l and in the on-body case also on its height h above the tissue. A solution for this can be found in [30] as:

$$R_\mathrm{r} = \eta_0 \left(\frac{l}{\lambda}\right)^2 \cdot s(h), \tag{24}$$

with η_0 the impedance of free space, λ the wavelength and $s(h)$ the factor defining the dependency on the height h above the tissue. As evaluated in Sec. III, in the on-body far-field the fields can locally be approximated by a plane wave. Thus, the incoming wave's power density becomes:

$$W_\mathrm{i} = \frac{E_\mathrm{i}^2}{2\eta_0}. \tag{25}$$

This reduces the expression for the on-body effective area of a normal Hertzian dipole to:

$$A_\mathrm{e,B} = \frac{\lambda^2}{4\pi s(h)}. \tag{26}$$

To calculate the on-body gain of the normal Hertzian dipole, its radiated E-field in the on-body far-field can be approximated by:

$$E = \frac{p \gamma_0 \eta_0}{4\pi R} \cdot 2F(\rho). \tag{27}$$

The electric dipole moment p can be related to the accepted power P_in using the relationships in [30] as:

$$p = \omega \sqrt{\frac{P_\mathrm{in} 8\pi\varepsilon_0}{c_0 \gamma_0^4 s(h)}}. \tag{28}$$

According to (19) this leads to the on-body gain of a normal Hertzian dipole as:

$$G_\mathrm{B} = s^{-1}(h). \tag{29}$$

Finally, the effective area of the isotropic antenna (21) for the derived on-body antenna parameters is calculated as the ratio between the effective area (26) and gain (29) of the Hertzian dipole.

APPENDIX B
ON-BODY GREEN'S FUNCTIONS

In the following the on-body Green's functions as discussed in Sec. II-A are listed. Here, the far-field approximation $|\gamma_0 R_1| \gg 1$ from [31] was used, which is sufficient for the necessary NF-FF transformation during the calculation of the on-body antenna parameters. The complete version valid also in the near-field can be derived from the solutions in [23].

$$a_0 = \begin{cases} z - h & \text{if } h > 0, \\ z & \text{if } h \leq 0. \end{cases} \tag{30}$$

$$a_1 = \begin{cases} z + h & \text{if } h > 0, \\ z & \text{if } h \leq 0. \end{cases} \tag{31}$$

$$R_n = \sqrt{\rho^2 + a_n^2} \tag{32}$$

$$S_n = \frac{a_n}{\sqrt{a_n^2 + \rho^2}} \tag{33}$$

$$C_n = \frac{\rho}{\sqrt{a_n^2 + \rho^2}} \tag{34}$$

$$Q_n = \begin{cases} R_n^{-1} e^{-\gamma_0 R_n} & \text{if } h \geq 0, \\ R_n^{-1} e^{-\gamma_0 R_n + \gamma_1 h} & \text{if } h < 0. \end{cases} \tag{35}$$

$$A = \frac{1 + \Gamma_\perp}{2} + \frac{1 - \Gamma_\perp}{2} F(w) \tag{36}$$

$$k_\perp = \begin{cases} 1 & \text{if } h \geq 0, \\ \Delta_\mathrm{m}^2 & \text{if } h < 0. \end{cases} \tag{37}$$

Electric currents $\mathbf{J}$:

$$G_{\mathrm{J},\rho}^{\mathrm{E},\parallel} = -S_0^2 Q_0 + \left[\Gamma_\perp S_1^2 + (1 - \Gamma_\perp)\Delta_\mathrm{m}^2 F(w)\right] Q_1 \tag{38}$$

$$G_{\mathrm{J},\rho}^{\mathrm{E},\perp} = k_\perp S_0 C_0 Q_0 \tag{39}$$

$$+ k_\perp \left[\Gamma_\perp S_1 - (1 - \Gamma_\perp)\Delta_\mathrm{m} F(w)\right] C_1 Q_1 \tag{40}$$

$$G_{\mathrm{J},\phi}^{\mathrm{E},\parallel} = Q_0 + \left[1 - \frac{2}{\gamma_0 n^2 R_1}(1 + A + \gamma_1 R_1 S_1)\right] Q_1 \tag{41}$$

$$G_{\mathrm{J,z}}^{\mathrm{E},\parallel} = S_0 C_0 Q_0 - \left[\Gamma_\perp S_1 - (1 - \Gamma_\perp)\Delta_\mathrm{m} F(w)\right] C_1 Q_1 \tag{42}$$

$$G_{\mathrm{J,z}}^{\mathrm{E},\perp} = -k_\perp C_0^2 Q_0 - k_\perp \left[\Gamma_\perp + (1 - \Gamma_\perp) F(w)\right] C_1^2 Q_1 \tag{43}$$

Magnetic currents $\mathbf{M}$

$$G_{\mathrm{M},\rho}^{\mathrm{E},\parallel} = S_0 Q_0 + \left[\Gamma_\perp S_1 - (1 - \Gamma_\perp)\Delta_\mathrm{m} F(w)\right] Q_1 \tag{44}$$

$$G_{\mathrm{M},\phi}^{\mathrm{E},\parallel} = -S_0 Q_0 \tag{45}$$

$$- \left[S_1 + \frac{2}{n}\left(S_1^2 - \frac{1}{\gamma_0 R_1}(1 + A - 3S_1^2)\right)\right] Q_1 \tag{46}$$

$$G_{\mathrm{M},\phi}^{\mathrm{E},\perp} = k_\perp C_0 Q_0 - k_\perp \left[1 - \frac{2}{\gamma_0 n^2 R_1}(1 + \gamma_1 R_1 S_1)\right] C_1 Q_1 \tag{47}$$

$$G_{\mathrm{M,z}}^{E,\parallel} = C_0 Q_0 + \left[\Gamma_\perp + (1 - \Gamma_\perp) F(w)\right] C_1 Q_1 \tag{48}$$

Copyright (c) 2021 IEEE. Personal use is permitted. For any other purposes, permission must be obtained from the IEEE by emailing pubs-permissions@ieee.org.

This is the author's version of an article that has been published in this journal. Changes were made to this version by the publisher prior to publication.
The final version of record is available at http://dx.doi.org/10.1109/TAP.2021.3060944

REFERENCES

[1] "IEEE standard for definitions of terms for antennas," *IEEE Std 145-2013 (Revision of IEEE Std 145-1993)*, pp. 1–50, 2014.

[2] K. Ali, F. Keshmiri, A. Brizzi, Y. Hao, and C. Craeye, "Body area networks at radio frequencies: Creeping waves and antenna analysis," *Comptes Rendus Physique*, vol. 16, no. 9, pp. 789–801, Nov. 2015. doi: 10.1016/j.crhy.2015.10.005. [Online]. Available: http://www.sciencedirect.com/science/article/pii/S1631070515001917

[3] M. Gallo, P. S. Hall, Q. Bai, Y. I. Nechayev, C. C. Constantinou, and M. Bozzetti, "Simulation and measurement of dynamic on-body communication channels," *IEEE Trans. Antennas Propag.*, vol. 59, no. 2, pp. 623–630, Feb. 2011. doi: 10.1109/TAP.2010.2093498

[4] T. Kumpuniemi, M. Hmlinen, K. Y. Yazdandoost, and J. Iinatti, "Human body shadowing effect on dynamic UWB on-body radio channels," *IEEE Antennas Wireless Propag. Lett.*, vol. 16, pp. 1871–1874, 2017. doi: 10.1109/LAWP.2017.2656246

[5] J. Naganawa, K. Wangchuk, M. Kim, T. Aoyagi, and J. Takada, "Simulation-based scenario-specific channel modeling for WBAN cooperative transmission schemes," *IEEE J. Biomed. Health Inform*, vol. 19, no. 2, pp. 559–570, 2015. doi: 10.1109/JBHI.2014.2326424

[6] T. Uusitupa and T. Aoyagi, "Analysis of dynamic on-body communication channels for various movements and polarization schemes at 2.45 GHz," *IEEE Trans. Antennas Propag*, vol. 61, no. 12, pp. 6168–6179, Dec. 2013. doi: 10.1109/TAP.2013.2281369

[7] Q. Wang, T. Tayamachi, I. Kimura, and J. Wang, "An on-body channel model for UWB body area communications for various postures," *IEEE Trans. Antennas Propag*, vol. 57, no. 4, pp. 991–998, Apr. 2009. doi: 10.1109/TAP.2009.2014526

[8] K. Ali, A. Brizzi, S. Lee, G. Yang, A. Alomainy, and Y. Hao, "Quantitative analysis of the subject-specific on-body propagation channel based on statistically created models," *IEEE Antennas Wireless Propag. Lett.*, vol. 14, pp. 398–401, 2015. doi: 10.1109/LAWP.2014.2362412

[9] N. P. B. Kammersgaard, S. H. Kvist, J. Thaysen, and K. B. Jakobsen, "Ear-to-ear propagation model based on geometrical theory of diffraction," *IEEE Trans. Antennas Propag*, vol. 67, no. 2, pp. 1153–1160, Feb. 2019. doi: 10.1109/TAP.2018.2882587

[10] A. Lea, P. Hui, J. Ollikainen, and R. G. Vaughan, "Propagation between on-body antennas," *IEEE Trans. Antennas Propag*, vol. 57, no. 11, pp. 3619–3627, Nov. 2009. doi: 10.1109/TAP.2009.2031917

[11] M. Grimm and D. Manteuffel, "On-body antenna parameters," *IEEE Trans. Antennas Propag*, vol. 63, no. 12, pp. 5812–5821, Dec. 2015. doi: 10.1109/TAP.2015.2482499

[12] D. Nikolayev, M. Zhadobov, and R. Sauleau, "Impact of tissue electromagnetic properties on radiation performance of in-body antennas," *IEEE Antennas and Wireless Propagation Letters*, vol. 17, no. 8, pp. 1440–1444, 2018. doi: 10.1109/LAWP.2018.2848943

[13] A. K. Skrivervik, M. Bosiljevac, and Z. Sipus, "Fundamental limits for implanted antennas: Maximum power density reaching free space," *IEEE Trans. Antennas Propag*, vol. 67, no. 8, pp. 4978–4988, 2019. doi: 10.1109/TAP.2019.2891697

[14] S. Kim, J. S. Ho, and A. S. Y. Poon, "Wireless power transfer to miniature implants: Transmitter optimization," *IEEE Trans. Antennas Propag*, vol. 60, no. 10, pp. 4838–4845, 2012. doi: 10.1109/TAP.2012.2207341

[15] L. Song and Y. Rahmat-Samii, "An end-to-end implanted brainmachine interface antenna system performance characterizations and development," *IEEE Trans. Antennas Propag*, vol. 65, no. 7, pp. 3399–3408, 2017. doi: 10.1109/TAP.2017.2700163

[16] D. U. Agu, M. Leece, J. Alcala-Medel, A. Sahdev, J. Lim, M. Olsen, B. Ngan, Y. Kim, and Y. Li, "Investigation of dominant wave mechanism and optimal antenna excitation for body-centric wireless propagations," *Progress In Electromagnetics Research C*, vol. 104, pp. 1–11, 2020. doi: 10.2528/PIERC20051605

[17] S. H. Kvist, J. Thaysen, and K. B. Jakobsen, "Ear-to-ear on-body channel model for hearing aid applications," *IEEE Trans. Antennas Propag*, vol. 63, no. 1, pp. 344–352, Jan. 2015. doi: 10.1109/TAP.2014.2368578

[18] T. Alves, B. Poussot, and J. Laheurte, "Analytical propagation modeling of BAN channels based on the creeping-wave theory," *IEEE Trans. Antennas Propag*, vol. 59, no. 4, pp. 1269–1274, Apr. 2011. doi: 10.1109/TAP.2010.2096184

[19] Z. Ma, J. Sarrazin, L. Petrillo, T. Mavridis, P. D. Doncker, and A. Benlarbi-Dela, "Antenna radiation characterization for on-body communication channel using creeping wave theory," in *2015 9th European Conference on Antennas and Propagation (EuCAP)*, Apr. 2015. ISSN 2164-3342 pp. 1–4.

[20] S. Razafimahatratra, J. Sarrazin, G. Valerio, F. Sarrazin, M. Casaletti, P. d. Doncker, and A. Benlarbi-Delai, "Input impedance of an aperture over a lossy half-space: Application to on-body antenna performance at 60 ghz," *Progress In Electromagnetics Research, PIER C*, vol. 83, pp. 161 – 178, Apr. 2018. [Online]. Available: https://hal.sorbonne-universite.fr/hal-01783831

[21] C. A. Balanis, *Antenna Theory: Analysis and Design*. USA: Wiley, 2016. ISBN 9781118642061

[22] K. A. Michalski and H.-I. Lin, "On the far-zone electromagnetic field of a vertical Hertzian dipole over an imperfectly conducting half-space with extensions to plasmonics," *Radio Science*, vol. 52, no. 7, pp. 798–810, 2017. doi: 10.1002/2017RS006299. [Online]. Available: https://agupubs.onlinelibrary.wiley.com/doi/abs/10.1002/2017RS006299

[23] P. R. Bannister, "Extension of finitely conducting earth-image-theory results to any range," Naval Underwater Systems Center New London Ct, Tech. Rep. NUSC-TR-6885, Jan. 1984. [Online]. Available: http://www.dtic.mil/docs/citations/ADA139144

[24] M. Grimm and D. Manteuffel, "Norton surface waves in the scope of body area networks," *IEEE Trans. Antennas Propag*, vol. 62, no. 5, pp. 2616–2623, May 2014. doi: 10.1109/TAP.2014.2307347

[25] R. Barake, A. Harmouch, and M. Kenaan, "Study on the validity of the formalism of norton to describe the propagation of electromagnetic waves on the surface of the body," *Journal of Communications Technology and Electronics*, vol. 61, no. 8, pp. 952–956, Aug. 2016. doi: 10.1134/S1064226916080039

[26] C. A. Balanis, *Advanced Engineering Electromagnetics, 2nd Edition*. Wiley, 2012. ISBN 9781118213483

[27] J. R. Wait, "The ancient and modern history of EM ground-wave propagation," *IEEE Antennas Propag. Mag.*, vol. 40, no. 5, pp. 7–24, Oct. 1998. doi: 10.1109/74.735961

[28] N. Chahat, G. Valerio, M. Zhadobov, and R. Sauleau, "On-Body Propagation at 60 GHz," *IEEE Trans. Antennas Propag*, vol. 61, no. 4, pp. 1876–1888, Apr. 2013. doi: 10.1109/TAP.2013.2242034

[29] N. P. B. Kammersgaard, S. H. Kvist, J. Thaysen, and K. B. Jakobsen, "Geometrical theory of diffraction formulation for on-body propagation," *IEEE Trans. Antennas Propag*, vol. 67, no. 2, pp. 1143–1152, Feb. 2019. doi: 10.1109/TAP.2018.2882596

[30] A. Sommerfeld and F. Renner, "Strahlungsenergie und Erdabsorption bei Dipolantennen," *Annalen der Physik*, vol. 433, no. 1, pp. 1–36, 1942. doi: 10.1002/andp.19424330102

[31] P. R. Bannister, "New formulas that extend Norton's farfield elementary dipole equations to the quasi-nearfield range," Naval Underwater Systems Center New London Ct, Tech. Rep. NUSC-TR-6883, Jan. 1984. [Online]. Available: http://www.dtic.mil/docs/citations/ADA139057

Copyright (c) 2021 IEEE. Personal use is permitted. For any other purposes, permission must be obtained from the IEEE by emailing pubs-permissions@ieee.org.

This is the author's version of an article that has been published in this journal. Changes were made to this version by the publisher prior to publication.
The final version of record is available at http://dx.doi.org/10.1109/TAP.2021.3060944

Lukas Berkelmann (S'17) was born in Stadthagen, Germany, in 1991. He received the B.Sc. and M.Sc. degrees in electrical engineering and information technology from the Leibniz University Hannover, Hannover, Germany, in 2014 and 2016, respectively. Since 2017 he has been a Research Assistant with the Institute of Microwave and Wireless Systems, Leibniz University Hannover. His current research is focused on the modeling of antennas and propagation for body-centric communication and EM modeling for biomedical applications.

Dirk Manteuffel (M'09) was born in Issum, Germany, in 1970. He received the Dipl.-Ing. and Dr.-Ing. degrees in electrical engineering from the University of Duisburg-Essen, Essen, Germany, in 1998 and 2002, respectively. From 1998 to 2009, he was with IMST, Kamp-Lintfort, Germany. As a Project Manager, he was responsible for industrial antenna development and advanced projects in the eld of antennas and EM modeling. From 2009 to 2016, he was a Full Professor of wireless communications at Christian-Albrechts-University, Kiel, Germany. Since June 2016, he is a Full Professor and the Director of the Institute of Microwave and Wireless Systems, Leibniz University Hannover, Hannover, Germany. His research interests include antenna integration and EM modeling for mobile communications and biomedical applications. Dr. Manteuffel was the recipient of the Young Scientist Award of the Vodafone Foundation for Science in 2004 for his research on the analysis and design of integrated mobile phone antennas with special emphasis on the interaction with the user.

Copyright (c) 2021 IEEE. Personal use is permitted. For any other purposes, permission must be obtained from the IEEE by emailing pubs-permissions@ieee.org.